It is generally accepted that ouabain modulates autonomic nerve function by inhibition of membrane Na^+,K^+-ATPase (Gillis & Quest 1979). This neuronal modulatory effect was mainly reported with *in vitro* sympathetic (Sweadner 1985), parasympathetic nerve endings (Satoh & Nakazato 1992, Gomez *et al.* 1996) and adrenal glands (Haass *et al.* 1997). Furthermore, ouabain-induced modulatory effect was reported with *in vitro* studies on motor endplate (Vyskocil & Illes 1977, Zemkova *et al.* 1990). From these *in vitro* studies, several mechanisms are presently suggested to induce release of neurotransmitter from the nerve endings. However, it is uncertain whether the manner of modulation differs between *in vivo* sympathetic and parasympathetic nerve endings. A major concern is whether ouabain induces a brisk increase in neurotransmitter efflux (spontaneous neurotransmitter release). Kranzhöfer *et al.* (1991) reported that ouabain-induced spontaneous noradrenaline (NA) release from sympathetic nerve endings. On the other hand, ouabain-induced spontaneous acetylcholine (ACh) release was reported *in vitro* studies using synaptosomes (Satoh & Nakazato 1992). No reports have described *in vivo* spontaneous ACh release evoked by ouabain. Further, a second issue is at which site ouabain induces neurotransmitter release: stored vesicle or axoplasma (Haass *et al.* 1997). NA and ACh release have been reported in stored vesicles and/or the axoplasma. It is uncertain, however, which site induces the predominant neurotransmitter release evoked by ouabain *in vivo*. Furthermore, the mechanisms underlying the neurotransmitter release evoked by ouabain remain unclear. Neuronal effects of ouabain have been attributed to the inhibitory action upon Na^+,K^+-ATPase and transmembrane sodium pump (Haass *et al.* 1997). As a consequence of the reduced sodium gradient at the plasma membrane, two possible mechanisms have been proposed to induce NA release from nerve endings; (i) carrier-mediated reversed NA transport, and (ii) Ca^{2+}-dependent exocytotic NA release. The manner and mechanisms of NA efflux have been extensively studied and accepted *in vivo* in isolated tissues (Sweadner 1985, Haass *et al.* 1997). However, it remains unclear whether these assumptions are valid in the cardiac sympathetic or parasympathetic nerve endings *in vivo*.

Cardiac dialysis technique in combination with highly sensitive measurement of NA or ACh has offered a powerful method for detecting the low level of dialysate NA or ACh obtained from the myocardial space (Akiyama *et al.* 1991, 1994). We demonstrated that dialysate NA or ACh levels were affected by local administration of pharmacological agents through dialysis probes, indicating that changes in dialysate NA or ACh levels reflect NA or ACh output from cardiac postganglionic sympathetic or parasympathetic nerve endings (Yamazaki *et al.* 1997, Kawada *et al.* 2001) respectively. Using dialysis technique, ouabain can be administered locally and it is possible to monitor NA or ACh output following locally applied ouabain (Yamazaki *et al.* 2001). Furthermore, comparison of the dialysate NA response in the presence and absence of neuronal agents can differentiate carrier-mediated NA release from calcium dependent exocytotic NA release (Yamazaki *et al.* 1997). With locally applied neuronal blockers, we examined the mechanisms and the sites underlying NA or ACh release evoked by ouabain.

Methods

Animal preparation

Adult cats were anaesthetized with pentobarbital sodium (30–35 mg kg^{-1} i.p.). The level of anaesthesia was maintained with a continuous intravenous infusion of pentobarbital sodium (1–2 mg kg^{-1} h^{-1}). The animals were intubated and ventilated with room air mixed with oxygen. Body temperature was maintained using a heated pad and lamp. All protocols were performed in accordance with the National Cardiovascular Center Research Institute Animal Care Ethics Committee guidelines that were in strict compliance with the NIH Guide for the Care and Use of Laboratory Animals. Electrocardiogram and mean arterial pressure were simultaneously monitored with a data recorder. The sixth rib on the left side was resected to expose the heart. With a fine guiding needle, one or two dialysis probes for dialysate sampling were implanted in the mid wall of the anterolateral region of the left ventricle. Heparin (100 U kg^{-1}) was administered after implantation of the dialysis probe and a maintenance dose was given every hour thereafter.

Dialysis technique

The material and properties of the dialysis probe were described previously (Akiyama *et al.* 1991, 1994). Briefly, we designed a transverse dialysis probe. Both ends of a dialysis fibre (13 mm length, 0.31 mm o.d. and 0.2 mm i.d.; PAN-1200, 50 000 molecular weight cutoff, Asahi Chemical, Tokyo, Japan) were connected and glued to polyethylene tubes (25 cm length, 0.5 mm o.d. and 0.2 mm i.d.). The dialysate NA or ACh levels were measured in separate animals. For the measurement of dialysate NA, the dialysis probe was perfused with Ringer's solution at 10 μL min^{-1}. Sampling periods were 2 min in duration (one sample volume = 20 μL), which was the minimum period necessary to collect sufficient NA for satisfactory measurement. For the measurement of dialysate ACh, Ringer's solution containing eserine (choline esterase

Journal compilation © 2007 Scandinavian Physiological Society, doi: 10.1111/j.1748-1716.2007.01749.x

inhibitor, 100 μM) was perfused at 2 μL min^{-1} and sampling periods were 15 min in duration. Dialysate sampling was started 120 min after probe implantation, when the dialysate NA or ACh concentration had reached a steady level. Each sample was collected in a microtube containing 0.1 N HCl or phosphate buffer to prevent oxidation. The dead-space volume between the dialysis and sample tube was measured. Taking this dead-space into account, samples were obtained.

Experimental protocols

In our previous study, we demonstrated that the dialysate NA or ACh levels reflect cardiac neuronal NA or ACh disposition at the nerve endings (Yamazaki *et al.* 1997, Kawada *et al.* 2001). Therefore, in the present study, we obtained dialysate samples and measured the dialysate NA or ACh levels as an index of NA or ACh output from post-ganglionic sympathetic or parasympathetic nerve endings respectively. Generally two mechanisms and sites are proposed to induce NA and ACh release from nerve endings: exocytotic (quantum) release from the stored vesicle and non-exocytotic (non-quantum) release from the axoplasma. The present studies were designed to clarify whether ouabain-induced NA or ACh efflux are affected by local administration of pharmacological agents that modify experimental conditions.

Protocol 1: Time courses of dialysate NA and ACh levels during local administration of ouabain. We examined the time course of dialysate NA and ACh levels during local administration of ouabain (100 μM). Ouabain was administered for 60 min. Dialysate NA levels were measured before and at 10-min intervals during ouabain administration. Dialysate ACh levels were collected in consecutive 15-min sampling periods.

Protocol 2: Influence of nerve transection and Na^+ channels on dialysate NA or ACh response evoked by ouabain. To test whether ouabain modulated central-mediated exocytotic neurotransmitter release, we examined the time course of ouabain-induced dialysate NA and ACh levels after transection of stellate ganglia or cervical parasympathetic nerve tract. For cardiac sympathetic denervation, the region of the stellate ganglia was exposed through the intercostal space, and bilateral transection of stellate ganglia was performed. After cardiac sympathetic denervation, heart rate response to carotid occlusion was blunted. In separate cats, cervical vagotomy was performed. We started dialysate sampling at 120 min after surgical interruption and ouabain-induced NA or ACh efflux was examined. Furthermore, to examine involvement of deporalization on NA or ACh release, ouabain-induced NA or ACh efflux was measured with addition of tetrodotoxin (TTX, 10 μM) through the dialysis probe. At 60 min after the beginning of TTX administration, we started the control sampling and examined the ouabain-induced NA or ACh response.

Protocol 3: Influence of NA-, ACh- and choline transporters on dialysate NA or ACh response evoked by ouabain. To test whether ouabain-induced neurotransmitter efflux was derived from axoplasma or stored vesicle, ouabain-induced NA or ACh efflux was examined with local administration of pharmacological agents, which affected the transport and content of neurotransmitter at the nerve endings. Membrane carrier-mediated NA transport was blocked by local administration of desipramine, whereas vesicular NA import was blocked by local administration of reserpine. In either case, ouabain-induced NA efflux was examined with the addition of desipramine (100 μM) or reserpine (10 μM) through the dialysis probe. The dosage of agent-administration was decided after referring to the previous studies (Akiyama *et al.* 1994, Yamazaki *et al.* 1997). Membrane carrier-mediated choline transport was blocked by local administration of hemicholinium-3 (10 μM), whereas vesicular ACh import was blocked by local administration of vesamicol (10 μM) (Kawada *et al.* 2001). In either case, ouabain-induced ACh efflux was examined with the addition of hemicholinium-3 or vesamicol through the dialysis probe.

Protocol 4: Influence of Ca^{2+} transporter, channel, mobilization on dialysate NA or ACh response evoked by ouabain. To test the contention that ouabain-induced neurotransmitter efflux was modulated by changes in intracellular Ca^{2+} levels, the influence of Ca^{2+} transporter, channel, mobilization on the dialysate NA or ACh response evoked by ouabain was examined. We focused on the involvement of three types of voltage-dependent Ca^{2+} channel, the L- and N types in the NA release evoked by ouabain. Sixty minutes after starting local administration of verapamil (100 μM), or ω-conotoxin GVIA (10 μM), we measured the ouabain-induced NA response. Second, we examined the involvement of plasma membrane Na^+/Ca^{2+} exchanger in the NA release evoked by ouabain. The inhibitors of membrane Na^+/Ca^{2+} exchange (dechlorobezamil; 100 μM, or KB7943; 10 μM) were locally administered through the dialysis probe and the ouabain-induced NA response was measured. Third, we examined the involvement of intracellular Ca^{2+} level in the NA release evoked by ouabain. An intracellular Ca^{2+} antagonist [3,4,5-trimethoxybenzoic acid 8-(dietyl amino)-octyl ester (TMB-8)] blocks the efflux of calcium from intracellular calcium stores without affecting influx

 doi: 10.1111/j.1748-1716.2007.01749.x

(Wiedenkeller & Sharp 1984). TMB-8 (1 mM) was locally administered through the dialysis probe and ouabain-induced NA response was measured. A similar pharmacological intervention was performed and ouabain-induced ACh responses were measured. Sixty minutes after starting local administration of verapamil (100 μM), or ω-conotoxin GVIA (10 μM), ω-conotoxin MVIIC (10 μM), we measured the ouabain-induced ACh response. The inhibitor of membrane Na^+/Ca^{2+} exchange (KB7943; 10 μM) was locally administered through the dialysis probe and the ouabain-induced ACh response was measured. Third, an intracellular Ca^{2+} antagonist (TMB-8, 1 mM) was locally administered through the dialysis probe and ouabain-induced ACh response was measured.

Analytical procedure

Dialysate NA concentrations were measured by HPLC with electrochemical detection (HPLC-ECD; Eicom, Kyoto, Japan). An alumina procedure was performed to remove the interfering compounds from the dialysate. The detection limit was 50 fmol per injection. Dialysate ACh concentration was measured directly by another HPLC-ECD. The detection limit was 50 fmol per injection. Details of HPLC-ECD for the NA and ACh measurements have been described elsewhere (Akiyama *et al.* 1991, 1994).

At the end of each experiment, the cats were killed with an overdose of pentobarbital sodium, and the implant sites were checked to confirm that the dialysis probes had been implanted within the left ventricular myocardium. Statistical analysis of the data was performed by analysis of variance (ANOVA). Statistical significance was defined as $P < 0.05$. Values are presented as mean ± SE.

Results

Protocol 1: Time course of dialysate NA and ACh levels during local administration of ouabain

Although local administration of ouabain did not affect haemodynamic parameters including heart rate, mean arterial pressure and electrocardiogram, ouabain induced the efflux of NA. Figure 1 (upper panel) shows the time course of the dialysate NA levels during local administration of ouabain (100 μM). Dialysate NA level increased significantly from 0.18 ± 0.06 nmol L^{-1} at control to 2.39 ± 0.53 nmol L^{-1} at 10, 12.92 ± 1.39 nmol L^{-1} at 20 min and 14.79 ± 1.97 nmol L^{-1} at 30 min. Subsequently, a slow decline occurred but high dialysate NA levels were maintained during locally applied ouabain. Peak level of dialysate NA ranged from 20 to 30 min after the beginning of ouabain administration. Figure 1 (lower panel) shows the time course of the dialysate ACh levels during local administration of ouabain (100 μM). Dialysate ACh level increased significantly from 0.91 ± 0.05 nmol at control to 3.6 ± 0.60 nmol L^{-1} at 0–15, 8.1 ± 1.4 nmol L^{-1} at 15–30 min and 6.8 ± 1.25 nmol L^{-1} at 30–45 min. Peak level of dialysate ACh appeared at 15–30 min after the beginning of ouabain administration.

Protocol 2: Influence of denervation and TTX on dialysate NA and ACh responses evoked by ouabain

We sampled the dialysates over 60 min of ouabain administration. To compare ouabain-induced NA or ACh levels under various interventions, ouabain-induced dialysate NA or ACh levels were subtracted from the control values. The sum of relative changes in dialysate NA or ACh (the unit: Σnmol/L) was expressed as an index of total NA or ACh release evoked by ouabain. Figure 2 (upper panel) shows the total NA release evoked by ouabain when cardiac sympathetic nerves were either intact, transected, pretreated with TTX. The ouabain-induced total NA release did not differ among them. Figure 2 (lower panel) shows the total ACh release evoked by ouabain when cardiac parasympathetic nerves were either intact, transected, or pretreated with TTX. The ouabain-induced total ACh release did not differ between the intact cardiac parasympathetic nerve and denervated groups whereas addition of TTX significantly inhibited the total ACh release by approx. 57% of vehicle.

Protocol 3: Influence of transport blocking agents on dialysate NA and ACh responses evoked by ouabain

Figure 3 (upper panel) shows the total NA release evoked by ouabain among various pharmacological interventions. Pretreatment with reserpine caused significant augmentation of the ouabain-induced total NA release whereas pretreatment with desipramine caused significant suppression of the total NA release. Figure 3 (lower panel) shows the total ACh release evoked by ouabain among various pharmacological interventions. The ouabain-induced total ACh release did not differ between the intact and hemicholinium-3 pretreated groups whereas addition of vesamicol significantly inhibited the total ACh release by approx. 45% of vehicle.

Protocol 4: Influence of Ca^{2+} mobilization on dialysate NA and ACh responses evoked by ouabain

Figure 4 (upper panel) shows the total NA release evoked by ouabain among various Ca^{2+} interventions. The total NA release in the 60 min after administration

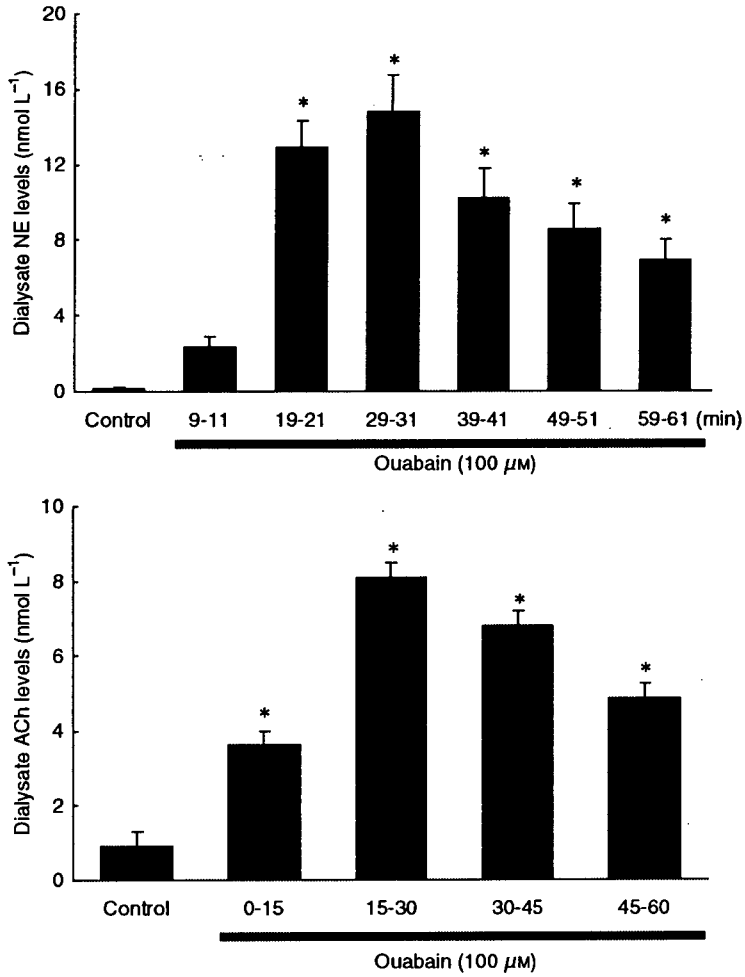

Figure 1 Upper panel: Time course of dialysate noradrenaline (NA) levels during local administration of ouabain (100 μM). Ouabain increased the dialysate NA levels. Subsequently, a slow decline occurred but high NA levels were maintained. Lower panel: Time course of dialysate acetylcholine (ACh) levels during local administration of ouabain (100 μM). Ouabain increased the dialysate ACh levels. Subsequently, a slow decline occurred but high ACh levels were maintained. Values are presented as the mean ± SE (for each column $n = 6$) *$P < 0.05$ vs. control.

of ouabain was significantly suppressed by approx. 47% and 55% of vehicle by addition of verapamil and ω-conotoxin GVIA. Pretreatment with TMB-8 caused significant suppression of the ouabain-induced total NA release whereas pretreatment with neither KB-7943 nor dechlorobezamil altered the total NA release. Figure 4 (lower panel) shows the total ACh release evoked by ouabain among various Ca^{2+} interventions. The total ACh release in the 60 min after administration of ouabain was significantly suppressed by approx. 57% of vehicle by addition of ω-conotoxin MVIIC. Pretreatment with neither verapamil nor ω-conotoxin GVIA altered the total ACh release. Pretreatment with TMB-8 caused significant suppression of the ouabain-induced total ACh release whereas pretreatment with KB-7943 did not alter the total ACh release.

Discussion

The present study indicates that in an *in vivo* preparation, ouabain alone induced NA or ACh release from sympathetic or parasympathetic nerve endings respectively. This discussion addresses mainly similarities and differences in ouabain alone induced NA or ACh releasing sites and mechanisms.

Regional depolarization evoked by ouabain

At the post-ganglionic nervous endings, ouabain induced NA and ACh release. The transection of sympathetic or parasympathetic nerve did not affect the amount of NA or ACh release evoked by ouabain. After the transection of cardiac sympathetic or parasympathetic nerves, ouabain at 100 μM induced increases in dialysate NA or ACh levels, which were as much as those evoked by electrical stimulation of the autonomic nerve (Akiyama *et al.* 1994, Yamazaki *et al.* 1997). These data suggest that ouabain itself induces regional depolarization following exocytosis. In the case of locally administered ouabain, ouabain produced intracellular Na^+ accumulation evoked by the inhibition of Na^+,K^+-ATPase (Mclvor & Cummings 1987).

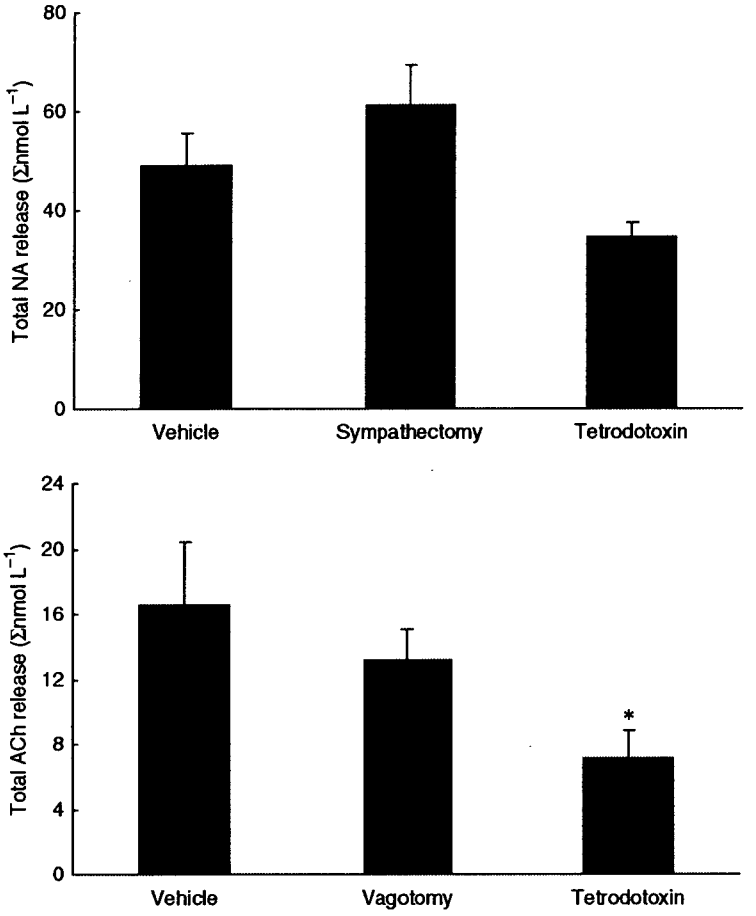

Figure 2 Upper panel: Ouabain-induced dialysate noradrenaline (NA) release in vehicle, cardiac sympathetic denervated and tetrodotoxin pretreated groups. Total NA release evoked by ouabain did not differ among the three groups. Lower panel: Ouabain-induced dialysate acetylcholine (ACh) release in vehicle, cardiac vagal denervated and tetrodotoxin pretreated groups. Total ACh release evoked by ouabain was suppressed by the pretreatment with tetrodotoxin. Values are presented as the mean ± SE (for each column $n = 6$). $^*P < 0.05$ vs. vehicle.

Regional depolarization may occur because of intracellular Na^+ accumulation (Calabresi *et al.* 1999, Dierkes *et al.* 2006). Similar finding was observed on motor endplate (Zemkova *et al.* 1990). Ouabain can increase the spontaneous ACh release by progressive decline in membrane potential when Na^+ pump is inhibited. If regional depolarization does indeed induce ACh or NA release via exocytosis from the stored vesicle, then pretreatment with TTX could inhibit this response. Local administration of TTX markedly inhibits ACh release whereas it only slightly inhibits the NA release evoked by ouabain. These results indicate that ouabain caused regional depolarization and exocytotic ACh release at the parasympathetic nerve endings. This conclusion is consistent with *in vitro* studies reported by Satoh & Nakazato (1992), and raises the question as to why TTX inhibited the ACh release but not the NA release evoked by ouabain. In the case of NA efflux evoked by ouabain, intracellular Na^+ accumulation may lead to a reduction in the Na^+ gradient between the intracellular and extracellular spaces. This reduced Na^+ gradient may cause carrier-mediated outward NA transport from axoplasma (Sharma *et al.* 1980). The threshold for intracellular Na^+ accumulation coupled to carrier-mediated outward NA transport might be lower than that for regional depolarization. Thus Na^+ accumulation coupled to regional depolarization may occur at the parasympathetic nerve endings but not at the sympathetic nerve endings.

The sites of neurotransmitter efflux evoked by ouabain

In general, two possible sites (the stored vesicle and axoplasma) were proposed to derive efflux of neurotransmitter at the nerve endings (Smith 1992, Vizi 1998). In the cholinergic nerve endings, a quantum amount of ACh was released from the stored vesicle via depolarization. Furthermore, a non-quantum amount of ACh seems to be leaked from the axoplasma without ACh transporter (Nikolsky *et al.* 1991). Local administration of vesamicol suppressed the ACh efflux evoked by ouabain. In contrast, local administration of hemicholinium-3 did not affect the ACh efflux evoked by ouabain. These data suggested that the ACh efflux was predominantly derived from the stored vesicle. This finding is consistent with the above-mentioned

Journal compilation © 2007 Scandinavian Physiological Society, doi: 10.1111/j.1748-1716.2007.01749.x

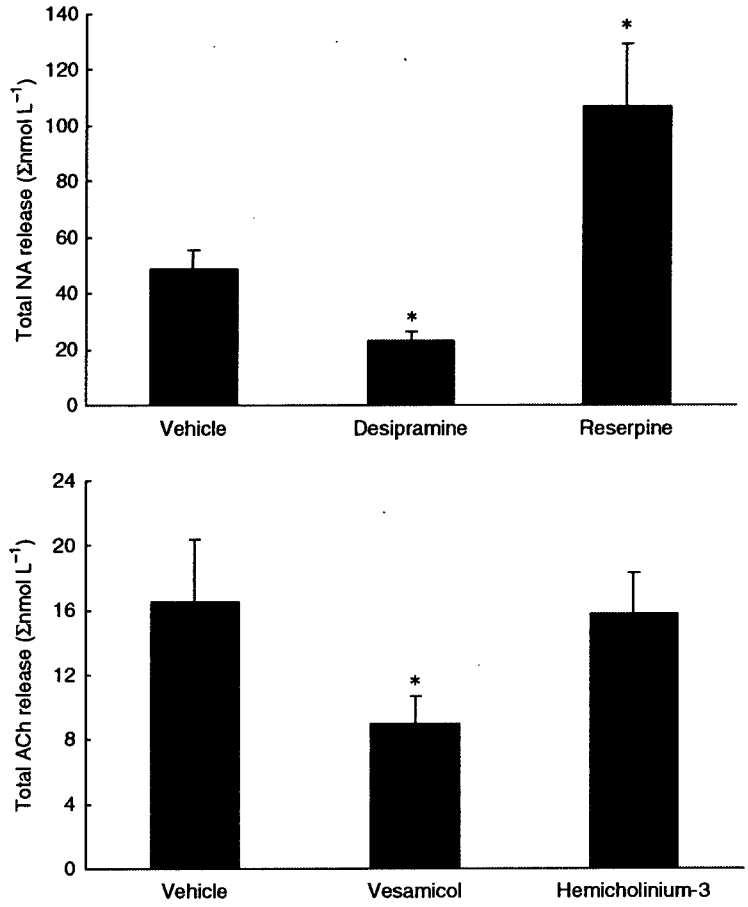

Figure 3 Upper panel: Ouabain-induced dialysate noradrenaline (NA) release among vehicle, desipramine and reserpine pretreated groups. Total NA release evoked by ouabain was suppressed by the pretreatment with desipramine and augmented by that with reserpine. Lower panel: Ouabain-induced dialysate acetylcholine (ACh) release in vehicle, vesamicol and hemicholinium-3 pretreated groups. Total ACh release evoked by ouabain was suppressed by the pretreatment with vesamicol. Values are presented as the mean ± SE (for each column $n = 6$). $^*P < 0.05$ vs. vehicle.

mechanism. Our data did not rule out the possibility of ACh efflux from the axoplasma. Vesamicol lowered the non-quantum ACh release by blocking the incorporated vesicle transporter in the terminal membrane (Edward *et al.* 1985). This involvement seems to be smaller than the involvement of ACh efflux from the stored vesicle.

Previous studies suggested that two different mechanisms (exocytosis and carrier-mediated outward transport) contributed to the amount of NA efflux evoked by ouabain (Kranzhöfer *et al.* 1991, Haass *et al.* 1997). The exocytotic NA release derived from the stored vesicle, whereas NA transporter carried out NA from the axoplasmic site via a reduced Na^+ gradient. However, it is uncertain which mechanism is predominantly involved in ouabain-induced NA efflux. To examine which site predominantly induced the neurotransmitter efflux evoked by ouabain, we administered vesicle and membranous amine transport blockers, which affected the neurotransmitter efflux evoked by ouabain. If NA efflux predominantly derives from the axoplasmic site, reserpine could increase axoplasmic NA level and augment the outward NA transport evoked by ouabain. Furthermore, as desipramine impairs carrier-mediated NA transport in both directions, desipramine could block NA efflux. NA release evoked by ouabain was augmented by local administration of reserpine but suppressed by desipramine. These data support the contention that ouabain-induced NA efflux is predominantly derived from the axoplasmic site.

Involvement of Ca^{2+} on ouabain-induced neurotransmitter efflux

Most *in vitro* studies suggested that ouabain somehow increases intracellular Ca^{2+} levels at the nerve endings and synaptosomes (Katsuragi *et al.* 1994, Casali *et al.* 1995, Wasserstrom & Aistrup 2005). Ouabain-induced intracellular Na^+ accumulation could evoke an elevation of intracellular Ca^{2+} level via Ca^{2+} channel opening (Katsuragi *et al.* 1994), Ca^{2+} release from internal stores (Nishio *et al.* 2004), and/or Na^+/Ca^{2+} exchange (Verbny *et al.* 2002). Thus, the elevation of intracellular Ca^{2+} may be associated with NA or ACh release from the autonomic nerve endings. At the parasympathetic nerve endings, neither verapamil nor ω-conotoxin GVIA

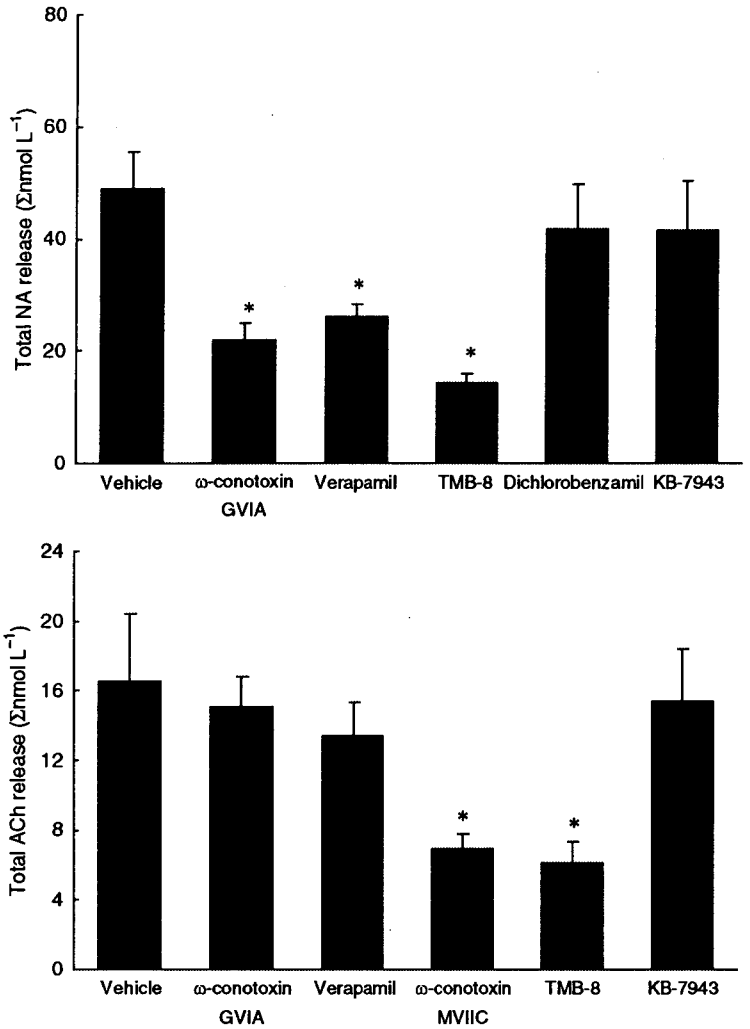

Figure 4 Upper panel: Ouabain-induced dialysate noradrenaline (NA) release in various Ca^{2+} interventions. Total NA release evoked by ouabain was suppressed by the pretreatment with ω-conotoxin GVIA, verapamil, TMB-8. Lower panel: Ouabain-induced dialysate acetylcholine (ACh) release in various Ca^{2+} interventions. Total ACh release evoked by ouabain was suppressed by the pretreatment with ω-conotoxin MVIICA or TMB-8. Values are presented as the mean ± SE (for each column $n = 6$). $^*P < 0.05$ vs. vehicle.

affected ACh release but ω-conotoxin MVIIC inhibited ACh release evoked by ouabain. Furthermore, KB-7943 did not affect either the ACh release evoked by ouabain. These data suggest that N or L-type Ca^{2+} channels or reversal Na^+/Ca^{2+} exchange might not be responsible for the ACh release evoked by ouabain. However, a marked suppression of ouabain-induced ACh release was observed with the addition of P/Q types channel blocker or TMB-8. In the case of parasympathetic nerve endings, Ca^{2+} elevation coupled to ACh release might be derived via internal stores or Ca^{2+} channels (P/Q types) rather than Na^+/Ca^{2+} exchange (Casali *et al.* 1995, Kawada *et al.* (in press)).

In the case of NA, ω-conotoxin GVIA or verapamil suppressed the NA release evoked by ouabain. Ouabain-induced NA release was independent of depolarization (TTX-resistant) but associated with the opening of Ca^{2+} channel. Furthermore, neither KB-7493 nor dichlorobenzamil affected the NA release evoked by ouabain. These data suggest that bi-directions of Na^+/Ca^{2+} exchange might not be responsible for the elevation of intracellular Ca^{2+} levels evoked by ouabain. A marked suppression of ouabain-induced NA release was observed with the addition of TMB-8. Taking these findings together, in the case of sympathetic nerve endings, Ca^{2+} elevation coupled to NA release might be derived via Ca^{2+} channels or internal store rather than membrane Na/Ca^{2+} exchange.

Although the type of Ca^{2+} channel for the NA or ACh release differed, involvement of cytosol Ca^{2+} in ouabain-induced neurotransmitter release did not differ between the parasympathetic and sympathetic nerve endings. However, the relation between TTX sensitive Na^+ channel and Ca^{2+} channel opening may differ between the parasympathetic and sympathetic nerve endings. In the present study, ouabain-induced NA efflux was suppressed by ω-conotoxin GVIA but not by TTX, indicating that TTX sensitive depolarization was not involved in Ca^{2+} channel opening coupled to exocytotic NA release. In contrast to NA release,

Journal compilation © 2007 Scandinavian Physiological Society, doi: 10.1111/j.1748-1716.2007.01749.x

ouabain-induced ACh release was suppressed by TTX and ω-conotoxin MVIIC, indicating that ouabain-induced depolarization and subsequently ACh release via P/Q type Ca^{2+} channel opening. TTX sensitive or resistant response may be interpreted as two different types of neurotransmitter release mechanisms. Alternatively, ouabain may have induced increases in intraneuronal Na^+ accumulation and elevation of extraneuronal K^+ levels by inhibition of Na^+,K^+-ATPase (D'Ambrosio *et al.* 2002). Elevations of both intracellular Na^+ and extracellular K^+ exerted regional depolarization following exocytosis via different mechanisms. In the previous study, we demonstrated that high K^+-induced NA release was insensitive to TTX but sensitive to ω-conotoxin GVIA. Furthermore, high K^+ caused a marked increase in dialysate NA but little increase in dialysate Ach (Yamazaki *et al.* 1998, Kawada *et al.* 2001). Thus high K^+-induced neurotransmitter release might greatly contribute to the increase in dialysate NA evoked by ouabain but might contribute little to the increase in dialysate ACh.

In conclusion, ouabain alone causes a brisk efflux of NA and ACh from cardiac sympathetic and parasympathetic nerve endings respectively. The ouabain-induced ACh release contributes to the mechanism of ACh exocytosis, which is triggered by centrally mediated or regional depolarization. The regional exocytosis is caused by opening of P/Q type Ca^{2+} channels and/or intracellular Ca^{2+} mobilization from the stored ACh vesicle. The ouabain-induced NA release contributes to the mechanisms of regional exocytosis and/or carrier-mediated outward transport of NA, from stored NA vesicle and/or axoplasma respectively. The regional exocytosis is caused by opening of N type Ca^{2+} channels and intracellular Ca^{2+} mobilization.

Conflict of interest

None.

This work was supported by Grants-in-Aid for scientific research (17591659) from the Ministry of Education, Culture, Sports, Science and Technology.

References

Akiyama, T., Yamazaki, T. & Ninomiya, I. 1991. *In vivo* monitoring of myocardial interstitial norepinephrine by dialysis technique. *Am J Physiol* **261**, H1643–H1647.

Akiyama, T., Yamazaki, T. & Ninomiya, I. 1994. *In vivo* detection of endogenous acetylcholine release in cat ventricles. *Am J Physiol* **266**, H854–H860.

Calabresi, P., Marfia, G.A., Centonze, D., Pisani, A. & Bernardi, G. 1999. Sodium influx plays a major role in the membrane depolarization induced by oxygen and glucose deprivation in rat striatal spiny neurons. *Stroke* **30**, 171–190.

Casali, T.A., Gomez, R.S., Moraes-Santos, T. & Gomez, M.V. 1995. Differential effects of calcium channel antagonists on tityustoxin and ouabain-induced release of [3H] acetylcholine from brain cortical slices. *Neuropharmacology* **34**, 599–603.

D'Ambrosio, R., Gordon, D.S. & Winn, H.R. 2002. Differential role of KIR channel and Na(+)/K(+)-pump in the regulation of extracellular K(+) in rat hippocampus. *J Neurophysiol* **87**, 87–102.

Dierkes, P.W., Wusten, H.J., Klees, G., Muller, A. & Hochstrate, P. 2006. Ionic mechanism of ouabian-induced swelling of leech Retzius neurons. *Pflugers Arch* **452**, 25–35.

Edward, C., Dolezal, D., Tucek, S., Zemkova, H. & Vyskocil, F. 1985. Is an acetylcholine transport system responsible for nonquantal release of acetycholine at the rodent myoneural junction? *Proc Natl Acad Sci USA* **82**, 3514–3518.

Gillis, R.A. & Quest, J.A. 1979. The role of the nervous system in the cardiovascular effects of digitalis. *Pharmacol Rev* **31**, 19–97.

Gomez, R.S., Gomez, M.V. & Prado, M.A.M. 1996. Inhibition of Na^+, K^+-ATPase by ouabain opens calcium channels coupled to acetylcholine release in guinea pig myenteric plexus. *J Neurochem* **66**, 1440–1447.

Haass, M., Serf, C., Gerber, S.H. *et al.* 1997. W. Dual effect of digitalis glycoside on norepinephrine release from human atrial tissue and bovine adrenal chromaffin cells: differential dependence on $[Na+]_i$ and $[Ca2+]_i$. *J Mol Cell Cardiol* **29**, 1615–1627.

Katsuragi, T., Ogawa, S. & Furukawa, T. 1994. Contribution of intra-and extracellular Ca^{2+} to noradrenaline exocytosis induced by ouabain and monesin from guinea-pig vas deferens. *Br J Pharmacol* **113**, 795–800.

Kawada, T., Yamazaki, T., Akiyama, T. *et al.* 2006. Effects of Ca2+ channel anatagonists on nerve stimulation-induced and ischemia-induced myocardial interstitial acetylcholine release in cats. *Am J Physiol* **291**, H2181–2191.

Kawada, T., Yamazaki, T., Akiyama, T. *et al.* 2001. *In vivo* assessment of acetylcholine-releasing function at cardiac vagal nerve terminals. *Am J Physiol* **281**, H139–H145.

Kranzhöfer, R., Haass, M., Kurz, T., Richardt, G. & Schömig, A. 1991. Effect of digitalis glycosides on norepinephrine release in the heart: dual mechanism of action. *Circ Res* **68**, 1628–1637.

McIvor, M.E. & Cummings, C.C. 1987. Sodium fluoride produces a K+ efflux by increasing intracellular Ca2+ through Na+-Ca2+ exchange. *Toxicol Lett* **38**, 169–176.

Nikolsky, E.E., Voronin, V.A. & Vyskocil, F. 1991. Kinetic differences in the effect of calcium on quantal and non-quantal acetylcholine release at the murine diaphragm. *Neurosci Lett* **123**, 192–194.

Nishio, M., Ruch, S.W., Kelly, J.E., Aistrup, G.L., Sheehan, K. & Wasserstrom, J.A. 2004. Ouabain increases sarcoplasmic reticulum calcium release in cardiac myocytes. *J Pharmacol Exp Ther* **308**, 1181–1190.

Satoh, E. & Nakazato, Y. 1992. On the mechanisim of ouabain-induced release of acetylcholine from synaptsomes. *J Neurochem* **58**, 1038–1044.

Sharma, V.K., Pottick, L.A. & Banerjee, S.P. 1980. Ouabain stimulation of noradrenaline transport in guinea pig heart. *Nature* **286**, 817–819.

 doi: 10.1111/j.1748-1716.2007.01749.x

Smith, D.O. 1992. Routes of actylcholine leakage from cytosolic and vesicular compartments of rat motor nerve terminals. *Neurosci Lett* **135**, 5–9.

Sweadner, K. 1985. Ouabain-evoked norepinephrine release from intact rat sympathetic neurons: evidence for carrier-mediated release. *J Neurosci* **5**, 2397–2406.

Verbny, Y., Zhang, C.L. & Chiu, S.Y. 2002. Coupling of calcium homeostasis to axonal sodium in axons of mouse optic nerve. *J Neurophysiol* **88**, 802–816.

Vizi, E.S. 1998. Differential temperature dependence of carrier-mediated (cytoplasmic) and stimulus-evoked (exocytotic) release of transmitter: a simple method to separate two types of relase. *Neurochem Int* **33**, 359–366.

Vyskocil, F. & Illes, P. 1977. Non-quantal release of transmitter at mouse neuromuscular junction and its dependency on the activity of Na^+-K^+ ATPase. *Pflugers Arch* **370**, 295–297.

Wasserstrom, J.A. & Aistrup, G.L. 2005. Digitalis: new actions for an old drug. *Am J Physiol Heart Circ Physiol* **289**, H1781–H1793.

Wiedenkeller, D.E. & Sharp, G.W. 1984. Unexpected potentiation of insulin release by the calcium store blocker TMB-8. *Endocrinolgy* **114**, 116–119.

Yamazaki, T., Akiyama, T., Kitagawa, H., Takauchi, Y., Kawada, T. & Sunagawa, K. 1997. A new, concise dialysis approach to assessment of cardiac sympathetic nerve terminal abnormalities. *Am J Physiol* **272**, H1182–H1187.

Yamazaki, T., Akiyama, T., Kawada, T. *et al.* 1998. Norepinephrine efflux evoked by potassium chloride in cat sympathetic nerves: dual mechanism of action. *Brain Res* **794**, 146–150.

Yamazaki, T., Akiyama, T. & Mori, H. 2001. Effects of nociceptin on cardiac norepinephrine and acetylcholine release evoked by ouabain. *Brain Res* **904**, 153–156.

Zemkova, H., Vyskocil, F. & Edwards, C. 1990. The effect of nerve terminal activity on non-quantal release of acetylcholine at the mouse neuromuscular junction. *J Physiol* **423**, 631–640.

Journal compilation © 2007 Scandinavian Physiological Society, doi: 10.1111/j.1748-1716.2007.01749.x

Polymer Journal, Vol. 39, No. 10, pp. 1065–1070 (2007)

Synthesis of Sugar-Polysiloxane Hybrids Having Rigid Main-Chains and Formation of their Nano Aggregates

Koutarou BEPPU,[1] Yoshiro KANEKO,[1] Jun-ichi KADOKAWA,[1,†]
Hidezo MORI,[2] and Takehiro NISHIKAWA[2]

[1]*Department of Nano-structured & Advanced Materials, Graduate School of Science and Engineering, Kagoshima University, 1-21-40 Korimoto, Kagoshima 890-0065, Japan*
[2]*National Cardiovascular Center Research Institute, 5-7-1, Fujishirodai, Suita 565-8565, Japan*

(Received March 22, 2007; Accepted July 12, 2007; Published August 28, 2007)

ABSTRACT: We synthesized sugar-polysiloxane hybrids having rigid main-chains by reaction of sugar-lactones with amine-functionalized polysiloxane (**1**). Reaction of gluconolactone (**2**) with **1** was performed to obtain polysiloxane (**3**) having polyol moieties derived from glucose. This material has the regularly controlled higher-ordered structure in solid state such as the hexagonal phase. A hydrophilic sugar-polysiloxane hybrid (**5**) was prepared by reaction of lactobionolactone (**4**) with **1**. Furthermore, an amphiphilic sugar-polysiloxane hybrid (**8**) was synthesized by introduction of stearoyl groups in addition to sugar groups on the surface of **1**. The SEM image of the amphiphilic material **8** exhibited formation of nano aggregates having the particle diameters of *ca.* 50 nm in water.
[doi:10.1295/polymj.PJ2006268]
KEY WORDS Glycopolymer / Sugar-lactone / Polysiloxane / Amphiphilic / Hybrid / Nano Aggregate /

There has been a growing interest in sugar portions of the glycoproteins because of exhibiting to bind to carbohydrate-recognition proteins, toxins, viruses, and cells. It has been known that a molecular assembly formed from the sugar-residues in the living system expresses stronger recognition ability than that of a single sugar molecule. This, so-called multivalent or cluster effect, has become a principle in the design of artificial glycoconjugate ligands. Therefore, polymeric materials having such functional sugar-residues, *i.e.*, 'glycopolymer', have widely been investigated because these materials efficiently show the multivalent effect.[1] So far, a number of such glycopolymers have been synthesized, which are composed of various organic polymer main-chains combined with a variety of sugar side-chains.[2–6]

Inorganic polymers such as polysiloxanes have various of interesting properties, *e.g.*, high oxygen permeability, low toxicity, and biocompatibility, which are advantages as biomaterials. Therefore, sugar-polysiloxane hybrids would be expected to have a significant potential for biological applications. In previous study, synthesis of such sugar-inorganic hybrids, composed of polydimethylsiloxane main-chain has been reported.[7–10] Since the main-chain has relatively flexible nature, nanostructures of the hybrid materials have not been controlled well.

Based on the above viewpoints, we paid attention to amine-functionalized polysiloxanes[11,12] for the main-chain of new sugar-polysiloxane hybrids, which were prepared by sol-gel reaction of amine-functionalized organoalkoxysilanes in strong acid aqueous solutions. The materials have rigid structures and construct hexagonal phase in solid state, because their frameworks are Si-O-Si network structures derived from trifunctional organoalkoxysilane. Furthermore, the materials are soluble in water and have reactive amino groups on the surface. Their rigidity, solubility, and reactivity would be advantageous properties to controlling nanostructures and introduction of various functional groups on the surface, in addition to the general characteristics of the inorganic polymers.

In previous communication, we briefly reported simple preparation method for a rigid polysiloxane hybrid (**3**) having polyol moieties using the amine-functionalized polysiloxane (**1**) and gluconolactone (**2**) (Scheme 1).[13] Because the sugar lactones like **2** react with the amino groups without protection of the hydroxy groups, they are useful substrates for such the simple procedure to exclude multi-reaction steps. However, **2** was not suitable for preparation of materials containing the sugar substituents, because the ring-opened moieties like the side chain of **3** formed from **2** had no any sugar-residues. Therefore, we have been carrying out studies on the synthesis of sugar-functionalized polysiloxane hybrids using disaccharide-lactone such as lactobionolactone (**4**), because the existence of sugar-residues can be maintained in spite of opening the lactone ring of **4** by the reaction with **1**.

†To whom correspondence should be addressed (Tel: +81-99-285-7743, Fax: +81-99-285-3253, E-mail: kadokawa@eng.kagoshima-u.ac.jp).

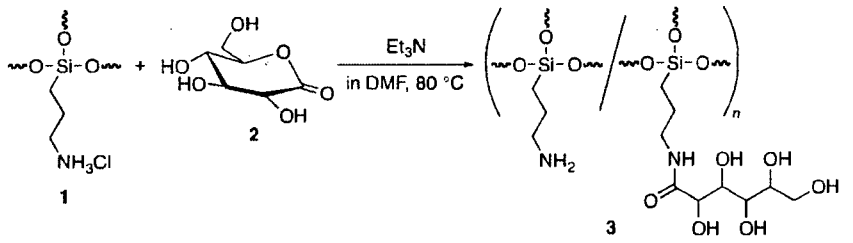

Scheme 1.

In this paper, we describe the synthesis of sugar-polysiloxane hybrids having rigid main-chains by the reaction of sugar-lactones with **1**. Furthermore, we prepared an amphiphilic sugar-polysiloxane hybrid by introduction of long alkyl chains in addition to sugar-residues on the surface of **1** to promote the formation of the nano aggregates in water, expecting the multivalent effects.

EXPERIMENTAL

Materials

The polysiloxane **1** was prepared according to the literature procedure.[11] *N,N*-Dimethylformamide (DMF), dimethyl sulfoxide (DMSO), and triethylamine were purified by distillation. Other reagents were used as received.

Reaction of 1 with Gluconolactone 2[13]

To a suspension of **1** (0.147 g, 1.0 mmol unit) in DMF (2.5 mL) was successively added triethylamine (0.15 mL, 1.1 mmol) and a solution of **2** (0.891 g, 5.0 mmol) in DMF (10 mL) with vigorously stirring at 80 °C under argon. After the mixture was stirred further at that temperature for 13 h, the obtained product was isolated by filtration, washed with DMF and acetone, and then dried under reduced pressure at 40 °C to yield 0.191 g of the yellow-powdered **3**. ^{1}H NMR (600 MHz, D_2O): δ 4.38–4.26 (br, -C(=O)-C*H*-), δ 4.16–4.05 (br, -C(=O)CH(OH)C*H*-), δ 3.88–3.60 (br, -C*H*(OH)C*H*(OH)CH_2-), δ 3.41–3.10 and 3.06–2.91 (br, -NCH_2-), δ 1.88–1.45 (br, -NCH$_2$CH_2-CH$_2$Si-), δ 0.94–0.47 (br, -CH_2Si-).

Synthesis of Hydrophilic Sugar-Polysiloxane Hybrid (5)

To a suspension of **1** (0.147 g, 1.0 mmol unit) in DMSO (3.0 mL) was successively added triethylamine (0.34 mL, 2.4 mmol) and a solution of **4** (1.701 g, 5.0 mmol) in DMSO (10 mL) with vigorously stirring at 80 °C under argon, and the mixture was stirred further at that temperature for 2 h. The mixture became gradually homogeneous solution. The solution was poured into acetone (300 mL) to precipitate the powdered product. The precipitated product was isolated by filtration, successively washed with acetone, hydrochloric acid (HCl) methanol solution and methanol, and then dried under reduced pressure at 40 °C to yield 0.332 g of the light yellow-powdered **5**. ^{1}H NMR (600 MHz, D_2O): δ 4.65–4.50 (br, -OC*H*-(CH-)O-), δ 4.50–4.32 (br, -C(=O)C*H*(OH)-), δ 4.32–4.13 (br, -C(=O)CH(OH)C*H*(OH)-), δ 4.08–3.49 (br, -C*H*(O-)C*H*(OH)CH_2OH, -C*H*(OH)C*H*(OH)C*H*(OH)-C*H*(O-)CH_2OH), δ 3.40–3.12 (br, -C(=O)NHCH_2-), δ 3.12–2.87 (br, Cl·NH$_3$CH_2-), δ 1.95–1.43 (br, -NCH$_2$CH_2CH$_2$Si-), δ 0.93–0.50 (br, -CH_2Si-).

Synthesis of Stearoyl-Carrying Polysiloxane (7)

To a solution of **1** (0.440 g, 3.0 mmol unit) in water (10 mL) was successively added triethylamine (1.0 mL, 7.2 mmol) and a solution of stearoyl chloride (**6**) (0.182 g, 0.6 mmol) in DMF (30 mL) with vigorously stirring at room temperature, and the solution was stirred further at that temperature for 10 min. After 5 mol/L HCl aqueous solution (2.88 mL, 14.4 mmol) was added to this mixture and this solution was stirred further for 5 min, the solution was poured into acetone (300 mL) to precipitate the powdered product. The precipitated product was isolated by filtration, washed with acetone and chloroform, and then dried under reduced pressure at 40 °C to yield 0.437 g of the white-powdered **7**. ^{1}H NMR (600 MHz, DMSO-d_6-D_2O): δ 3.09–2.72 (br, -NCH_2-), δ 2.20–2.01 (br, -C(=O)CH_2-), δ 1.88–1.55 (br, -NCH$_2$CH_2-CH$_2$Si-), δ 1.50–1.40 (br, -C(=O)CH$_2$CH_2-), δ 1.28–1.10 (br, -CCH_2C-), δ 0.95–0.45 (br, -CH$_3$, -CH_2Si-).

Synthesis of Amphiphilic Sugar-Polysiloxane Hybrid (8)

To a solution of **7** (0.150 g, 1.3 mmol unit) in DMSO (5 mL) was successively added triethylamine (0.46 mL, 3.3 mmol) and a solution of **4** (2.212 g, 6.5 mmol) in DMSO (15 mL) with stirring at 80 °C, and the solution was stirred further at that temperature for 2 h. The solution was poured into acetone (300 mL) to precipitate the powdered product. The precipitated product was isolated by filtration, successively washed with acetone, HCl methanol solution and

methanol, and then dried under reduced pressure at 40 °C to yield 0.270 g of the light yellow-powdered **8**. ^{1}H NMR (600 MHz, DMSO-d_6-D_2O): δ 4.46–4.28 (br, -OC*H*(CH-)O-), δ 4.28–4.11 (br, -C(=O)C*H*-(OH)-), δ 4.11–3.95 (br, -C(=O)CH(OH)C*H*(OH)-), δ 3.90–3.28 (br, -C*H*(O-)C*H*(OH)CH_2OH, -C*H*(OH)-C*H*(OH)C*H*(OH)C*H*(O-)CH_2OH, overlapped with HOD signal), δ 3.28–2.96 (br, -C(=O)NHCH_2-), δ 2.96–2.70 (br, Cl·NH_3CH_2-), δ 2.20–2.01 (br, -C(=O)-CH_2-), δ 1.80–1.32 (br, -NCH_2CH_2CH_2Si-, -C(=O)-CH_2CH_2-), δ 1.28–1.13 (br, -CCH_2C-), δ 0.88–0.80 (br, -CH_3), δ 0.80–0.36 (br, -CH_2Si-).

Measurements

The IR spectra were recorded using a SHIMADZU FT/IR-8400 spectrometer. The ^{1}H NMR spectra (600 MHz) were recorded using a JEOL ECA600 spectrometer. The gel permeation chromatographic (GPC) analyses were performed by using a TOSOH CCPD with RI detector under the following conditions: Shodex GF-310 column with water as the eluent at a flow rate of 0.5 mL/min. The calibration curve was obtained using pullulan standards. The X-ray diffraction (XRD) measurements were conducted at a scanning speed of $2\theta = 0.2°$/min using a RINT 1200 (Rigaku Co., Ltd) diffractometer with Ni-filtered CuKα radiation ($\lambda = 0.15418$ nm). The scanning electron microscope (SEM) images were obtained using a Hitachi S-4100 electron microscope. The dynamic light scattering (DLS) measurement was performed on a Zetasizer 3000 (Malvern Instruments).

RESULTS AND DISCUSSION

Reaction of 1 with 2

As previously reported,[13] an introduction of **2** to **1** was performed by heating at 80 °C in the presence of triethylamine in DMF to prepare a rigid polysiloxane **3** having polyol moieties (Scheme 1). The obtained product **3** was soluble in water and DMSO, but insoluble in typical organic solvents such as methanol, acetone, chloroform, and *n*-hexane.

The IR spectrum of the product showed an absorption at 1150 cm^{-1} attributed to the Si-O bond of the polysiloxane, an absorption at 1080 cm^{-1} assigned to the C-O bond of the polyol moiety derived from **2**, and an absorption at 1650 cm^{-1} due to the C=O bond of the amido group. In addition, the ^{1}H NMR spectrum in D_2O of the product showed both signals due to **1** and **2**. Furthermore, a methylene signal (δ 3.41–3.10) neighboring the amido group was appeared at lower magnetic field compared with a signal (δ 3.06–2.91) neighboring the unreacted amino group. These spectroscopic results indicated that the product has the structure **3** connecting **1** with **2** by the covalent bonds. The functionality of **2** to **1** was calculated to be *ca.* 75% based on the integrated ratio of the methylene signal neighboring the amido group to the methylene signal neighboring the silicon atom.

The molecular weights of **3** and **1** were evaluated by GPC analyses with water as the eluent. The GPC peak of **3** was shifted to the range of higher molecular weight compared to that of **1**. The M_n values of **3** and **1** estimated using pullulan standards were 21,200 g/mol ($M_w/M_n = 1.33$) and 10,300 g/mol ($M_w/M_n = 1.41$), respectively.

The XRD profile of **3** showed three peaks with the *d*-value ratio of $1:1/\sqrt{3}:1/2$ assigned to the (100), (110), and (200) peaks, respectively, indicating that the product has a hexagonal phase. Additionally, the *d*-value of the (100) peak of **3** ($d = 1.76$ nm) was larger than that of **1** ($d = 1.41$ nm). This indicates that the hexagonal phase in solid state was maintained in spite of the increase in the *d*-value by introduction of **2** to **1**.

The above analytical data indicated that **2** efficiently reacted with the amino groups in **1**, giving rise to **3**. To introduce the sugar moieties such as galactose residues on the surface of **1** by means of this reaction manner, the following experiments were performed using lactobionolactone **4**.

Synthesis of Hydrophilic Sugar-Polysiloxane Hybrid 5

We investigated synthesis of galactose-functionalized polysiloxane hybrid **5** by the reaction of **4** with **1**. Procedures for synthesis of **5** were almost same as those of **3**. Since the reaction in DMF gave the insoluble product, however, we employed DMSO as the alternative solvent, which was favorable for this reaction system. When an introduction of **4** to **1** was performed by heating at 80 °C in the presence of triethylamine in DMSO (Scheme 2), the initial reaction system was heterogeneous, which gradually became homogeneous with progress of the reaction. After the product was isolated as the fraction insoluble in acetone, unreacted amino groups were converted to ammonium cations by addition of HCl methanol solution in order to increase solubility and stability of the product in water. The obtained product **5** was soluble in water and DMSO, but insoluble in typical organic solvents such as methanol, acetone, chloroform, and *n*-hexane.

The IR spectrum of the product showed absorptions at 1650 cm^{-1} attributed to the C=O bond of the amido group, indicating the introduction of **4** to **1**. The ^{1}H NMR spectrum in D_2O of the product in Figure 1 shows both signals derived from **1** and **4**. Furthermore, a methylene signal $\mathbf{H_c}$ neighboring the amido group appeared at lower magnetic field compared with a signal $\mathbf{H_{c'}}$ neighboring the unreacted amino group. These spectroscopic data support the structure **5** of

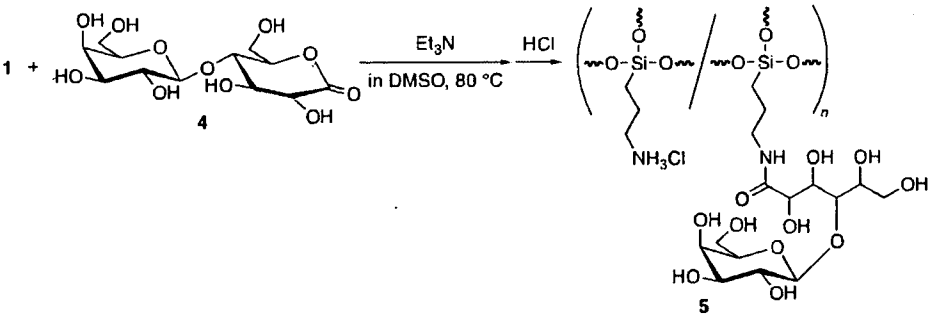

Scheme 2.

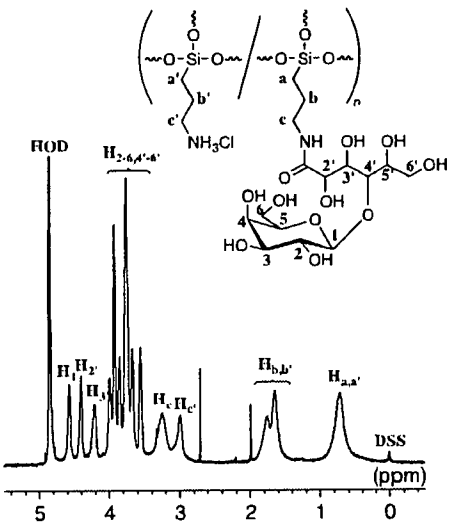

Figure 1. ^{1}H NMR spectrum of **5** in D_2O. Chemical shifts were referenced to sodium 2,2-dimethyl-2-silapentane-5-sulfonate (DSS) (δ 0.0 ppm).

the product. The functionality of **4** to **1** was calculated by the integrated ratio of the signal $\mathbf{H_1}$ to the signals $\mathbf{H_a}$ and $\mathbf{H_{a'}}$ in Figure 1 to be *ca.* 57%. Although the XRD profile of **3** showed three peaks for a typical hexagonal phase as described above, no diffraction peak was observed for **5**, indicating that a regular higher-ordered structure was not formed in the solid state. This would be because that the bulkiness of **4** affected the higher-ordered structure of **5**. However, **5** probably has the rigid structure in the solution due to the Si-O-Si network structure of the main-chain derived from trifunctional organoalkoxysilane. The molecular weight (M_n) of **5** estimated by GPC analysis with water as the eluent using pullulan standards was 44,700 g/mol (M_w/M_n = 1.44).

Synthesis of Amphiphilic Sugar-Polysiloxane Hybrid 8

To promote the formation of the nano aggregates of sugar-polysiloxane hybrid, we attempted synthesis of an amphiphilic hybrid **8** by introduction of the hydrophobic stearoyl groups in addition to the hydrophilic sugar groups on the surface of **5**. However, the reaction of **5** with stearoyl chloride **6** did not proceed to obtain **8**, probably due to bulkiness of sugar-residues existed on the surface of **5**. As an alternative reaction manner, an introduction of **6** to **1** was firstly carried out in the presence of triethylamine in water/DMF mixed solvent at room temperature to produce stearoyl-carrying polysiloxane **7** (Scheme 3). After addition of HCl aqueous solution to this reaction solution, the product was isolated as the fraction insoluble in acetone. The obtained product **7** was soluble in DMSO, but insoluble in water.

The IR spectrum of the product showed an absorption at 1640 cm^{-1} assigned to the C=O bond of the amido group. In addition, the ^{1}H NMR spectrum in DMSO-d_6 (including a small amount of D_2O) of the product in Figure 2 shows both signals derived from **1** and **6**. These spectroscopic results indicate the intro-

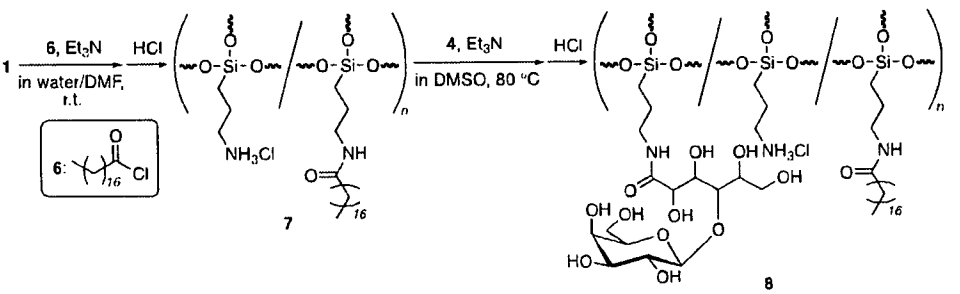

Scheme 3.

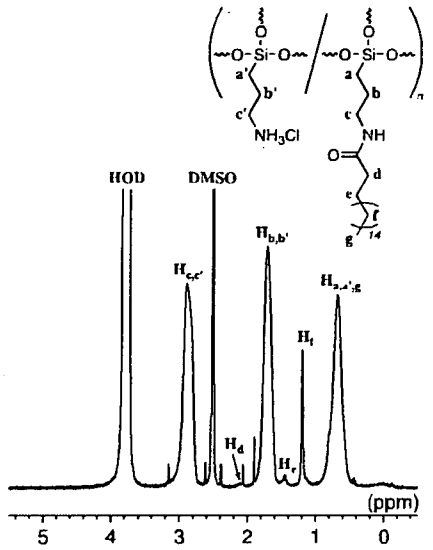

Figure 2. ^{1}H NMR spectrum of **7** in DMSO-d_6 (including a small amount of D_2O). Chemical shifts were referenced to DMSO (δ 2.5 ppm).

duction of **6** to **1**, leading to **7**. The functionality of **6** to **1** was calculated to be *ca.* 2% based on the integrated ratio of the signal $\mathbf{H_f}$ to the signal $\mathbf{H_b}$ and $\mathbf{H_{b'}}$. When the feed ratio of **6** to **1** was increased, the insoluble product was obtained.

As a second step, we carried out a reaction of **4** with **7** by heating at 80 °C in the presence of triethylamine in DMSO to obtain amphiphilic sugar-polysiloxane hybrid **8** (Scheme 3). The product was isolated as the fraction insoluble in acetone, followed by washing with acetone, HCl methanol solution, and methanol. The obtained product **8** was soluble in water and DMSO, but insoluble in typical organic solvents such as methanol, acetone, chloroform, and *n*-hexane.

The IR spectrum of the product showed an absorption at 1140 cm^{-1} attributed to the Si-O bond, an absorption at 1080 cm^{-1} assigned to the C-O bond of **4**, and an absorption at 1650 cm^{-1} due to the C=O bond of the amido group. Additionally, the ^{1}H NMR spectrum in DMSO-d_6 (including a small amount of D_2O) of the product in Figure 3a shows signals derived from **1**, **4**, and **6**. Furthermore, the methylene signals $\mathbf{H_a}$ and $\mathbf{H_b}$ of the product shift to higher field and the methylene signal $\mathbf{H_c}$ shifts to lower field compared with those of **7**. These shifts have also been observed in the synthesis of **3**,[13] and are attributed to progress of the amidation reaction of **7** with **4**. These spectroscopic results fully support the structure of the sugar- and stearoyl-functionalized polysiloxane **8**. The functionality of **4** to **1** was calculated by the integrated ratio of the signal $\mathbf{H_{f'}}$ to the signal $\mathbf{H_1}$ in Figure 3 to be *ca.* 48%, when the reaction was carried out under the conditions as described in experimental section.

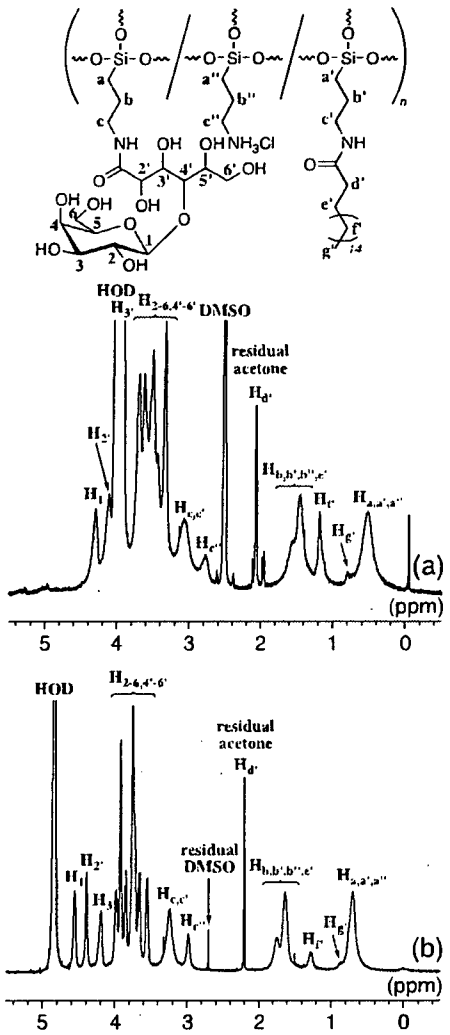

Figure 3. ^{1}H NMR spectrum of **8** (a) in DMSO-d_6 (including a small amount of D_2O) and (b) in D_2O. Chemical shifts were referenced to DMSO (δ 2.5 ppm) and DSS (δ 0.0 ppm), respectively.

The functionalities were variable by changing the feed ratio of **4** to **7**.

Interestingly, intensity of a signal $\mathbf{H_{f'}}$ due to stearoyl group of **8** in D_2O decreases compared with that in DMSO-d_6 (Figure 3b). This observation indicates that the stearoyl groups existed in the inside of the intra and intermolecular aggregates of **8** in D_2O. To confirm the formation of nano aggregates of **8** in water, SEM image of **8** was taken. The SEM specimen was prepared by evaporating an aqueous solution of **8** on a spinning aluminium plate. The SEM image of the surface of **8** coated on the aluminum plate shows that nano aggregates were formed from **8** (Figure 4); nano aggregates having the particle diameters of *ca.* 50 nm are appearing at high frequency and larger particles that represent a diameter of *ca.* 500 nm are coexisting with smaller aggregates at much lower frequency (a few aggregates in a SEM image). The particle size

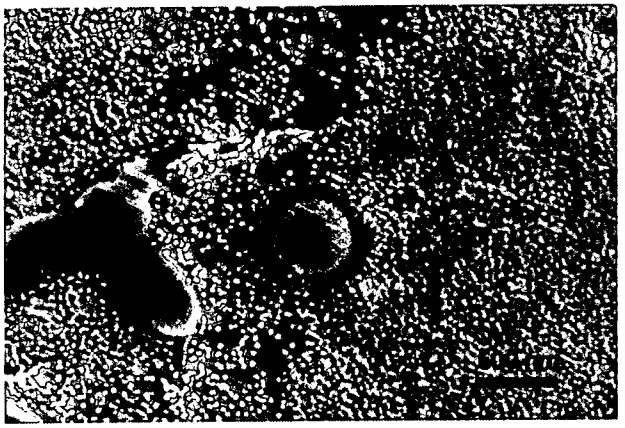

Figure 4. SEM image of **8**.

was also confirmed by dynamic light scattering (DLS) measurement. The mean diameter of the particle composed of **8** was 67.7 ± 4.5 nm (poly dispersity index: 0.273) in water. The aggregate size corresponds well to that was observed in the SEM image of the spin-coating sample of **8**.

CONCLUSIONS

The amino groups existed on the surface of the rigid polysiloxane (**1**) efficiently reacted with gluconolactone (**2**) to give the corresponding hybrid (**3**). This reaction manner was employed for preparation of the hydrophilic sugar-polysiloxane hybrid (**5**), which was achieved by the reaction of **1** with lactobionolactone (**4**). Furthermore, the amphiphilic sugar-polysiloxane hybrid (**8**) was also derived from **1** by the successive reactions with stearoyl chloride (**6**) and with **4**. The obtained hybrid materials **5** and **8** have galactose residues on their surfaces. Although hybrid **3** had the regular higher-ordered structure in the solid state, hydrophilic sugar-polysiloxane hybrid **5** did not form such a structure by the bulkiness of **4**. However, amphiphilic sugar-polysiloxane hybrid **8** formed the nano aggregates in water, which was confirmed by the ^{1}H NMR, SEM, and DLS analyses, expecting the multivalent effects of sugar-residues. The present materials are new class of sugar-inorganic hybrids, which have rigid polysiloxane main-chains.

Acknowledgment. The author (T.N.) thanks Dr. Tetsuji Yamaoka and Dr. Atsushi Mahara of National Cardiovascular Center for dynamic light scattering measurement.

REFERENCES

1. M. Okada, *Prog. Polym. Sci.*, **26**, 67 (2001).
2. K. Kobayashi, A. Tsuchida, T. Usui, and T. Akaike, *Macromolecules*, **30**, 2016 (1997).
3. X. L. Sun, K. M. Faucher, M. Houston, D. Grande, and E. L. Chaikof, *J. Am. Chem. Soc.*, **124**, 7258 (2002).
4. Q. Wang, J. S. Dordick, and R. J. Linhardt, *Chem. Mater.*, **14**, 3232 (2002).
5. A. B. Lowe, B. S. Sumerlin, and C. L. McCormick, *Polymer*, **44**, 6761 (2003).
6. L. Albertin, M. Stenzel, C. Barner-Kowollik, L. J. R. Foster, and T. P. Davis, *Macromolecules*, **37**, 7530 (2004).
7. G. Jonas and R. Stadler, *Acta. Polym.*, **45**, 14 (1994).
8. V. Braunmühl, G. Jonas, and R. Stadler, *Macromolecules*, **28**, 17 (1995).
9. V. Braunmühl and R. Stadler, *Polymer*, **39**, 1617 (1998).
10. K. Loos, G. Jonas, and R. Stadler, *Macromol. Chem. Phys.*, **202**, 3210 (2001).
11. Y. Kaneko, N. Iyi, K. Kurashima, T. Matsumoto, T. Fujita, and K. Kitamura, *Chem. Mater.*, **16**, 3417 (2004).
12. Y. Kaneko, N. Iyi, T. Matsumoto, and K. Kitamura, *Polymer*, **46**, 1828 (2005).
13. Y. Kaneko, J. Kadokawa, M. Setoguchi, and N. Iyi, *Polymer*, **46**, 8905 (2005).

JOURNAL OF BIOSCIENCE AND BIOENGINEERING
Vol. 103, No. 1, 98–100. 2007
DOI: 10.1263/jbb.103.98

High Inoculation Cell Density Could Accelerate the Differentiation of Human Bone Marrow Mesenchymal Stem Cells to Chondrocyte Cells

Mutsumi Takagi,[1]* Yousuke Umetsu,[1] Masashi Fujiwara,[1] and Shigeyuki Wakitani[2]

Division of Biotechnology and Macromolecular Chemistry, Graduate School of Engineering, Hokkaido University, N13W8, Kita-ku, Sapporo 060-8628, Japan[1] and Orthopedic Surgery, Osaka-City University School of Medicine, 1-4-3 Asahi-machi, Abeno-ku, Osaka, Osaka 545-8585, Japan[2]

Received 28 July 2006/Accepted 25 October 2006

The effects of the density of human mesenchymal stem cells (MSCs) on their differentioation to chondrocytes in a differentiation medium supplemented with dexamethasone, TGFβ3, and IGF-1 were investigated for the regenerative therapy of cartilage. The increase in the initial density of MSCs from 0.05×10^4 to 0.9×10^4 cells/cm^2 accelerated the increase in the expression level of aggrecan mRNA during the differentiation culture for 7 d. The conditioned medium harvested at 7 d from the differentiation culture with an initial MSC density of 0.3×10^4 cells/cm^2 accelerated the initial increase in the expression level for 3 d in the differentiation culture with an initial MSC density of 0.3×10^4 cells/cm^2, whereas the conditioned medium harvested at 7 d in the differentiation culture with an initial MSC density of 0.05×10^4 cells/cm^2 did not. The differentiation culture after 14 d with an initial MSC concentration of 0.3×10^4 cells/cm^2 showed an expression level 1.7-fold that in the case of the culture with an initial MSC concentration of 0.05×10^4 cells/cm^2. Thus, a high MSC inoculum density might be appropriate for the rapid differentiation of MSCs to chondrocytes.

[**Key words:** cell density, mesenchymal stem cell, differentiation, chondrocyte].

Combined addition of insulin-like growth factor (IGF)-1, transforming growth factor (TGF)-β3 and dexamethasone was effective for the differentiation of mesenchymal stem cells (MSCs) in adult bone marrow to chondrocyte cells (1). In general, cytokines produced by cultivated cells other than externally added cytokines to the culture, might affect cell differentiation. Thus, cell density should have some affect on cell differentiation because cytokine production rate depends on cell density. For example, an increase in initial stromal cell concentration from 0.4×10^5 to 2.7×10^5 cells/ml increased progenitor concentration during a three-dimensional coculture of murine bone marrow hematopoietic cells with murine bone marrow stromal cells (2). Moreover, initial cell density might be one of the easily adjustable operational variables.

Besides generally added cytokines such as TGF-β3 and IGF-1, cytokines secreted by MSCs have been considered to regulate the differentiation of MSCs to chondrocyte cells. However, it remains unclear how MSC density influences the differentiation of MSCs to chnodrocytes. Consequently, the effects of MSC density on MSC differentiation were investigated in this study.

MSCs were isolated from bone marrow aspirate obtained by routine iliac crest aspiration from human donors (age: 65–73) as previously reported (1). The content of $CD105^+$ $CD45^-$ cells among the cells analyzed by flowcytometer was approximately 90% (data not shown) (3).

The growth medium used was DMEM-LG (Gibco, NY, USA) supplemented with 10% FCS (Gibco), 2500 U/*l* penicillin, and 2.5 mg/*l* streptomycin.

The differentiation medium was DMEM-HG (Gibco) supplemented with 10% FCS, 2500 U/*l* penicillin, 2.5 mg/*l* streptomycin, 50 μg/ml L-ascorbic acid 2-phosphate (Wako Pure Chemicals, Osaka), 100 μg/ml sodium pyruvate (Wako), and 40 μg/ml proline (Wako). Growth factors, namely, 10 ng/ml TGF-β3 (Peprotech, Rocky Hill, NJ, USA), 39 ng/ml dexamethasone (ICN Biomedicals, Irvine, CA, USA), and 100 ng/ml insulin-like growth factor-I (IGF-I; Peprotech), were added.

The cells were cultured on a multiwell dish (9.6 cm^2; Sumitomo Bakelite, Tokyo) at densities of 0.05×10^4 to 0.9×10^4 cells/cm^2 employing the growth medium and allowed to attach for 1 d at 37°C in 5% CO_2. Then, the medium was replaced with the differentiation medium and differentiation culture was started. Cell density was determined by trypan blue dye exclusion after trypsinization.

The mRNA expression ratio of aggrecan, which is a typical extra cellular matrix produced by chondrocytes, to actin was determined by previously reported method emplying real-time RT-PCR (1) and employed as an index of differentiation of MSCs to chondrocytes.

* Corresponding author. e-mail: takagi-m@eng.hokudai.ac.jp
phone/fax: +81-(0)11-706-6567

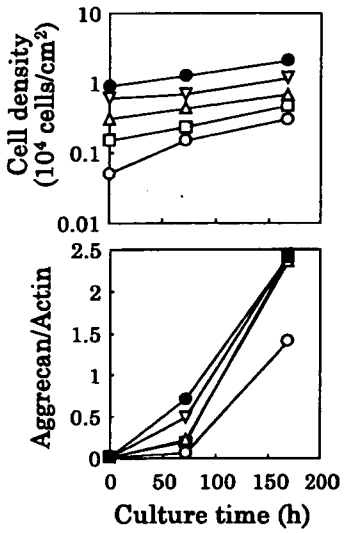

FIG. 1. Effect of initial cell density on expression level of aggrecan mRNA. Differentiation culture was performed for 7 d employing several inoculation cell densities of 0.05 (open circles), 0.15 (squares), 0.3 (triangles), 0.6 (inverted triangles), and 0.9 (closed circles) $\times 10^4$ cells/cm^2. The average of triplicate determinations is shown.

Differentiation culture was performed for 7 d employing several inoculation cell densities (0.05, 0.15, 0.3, 0.6, 0.9×10^4 cells/cm^2) and the expression level of aggrecan mRNA was determined (Fig. 1). The cells grew exponentially in all the cultures and there was almost no difference in specific cell growth rate between cultures that used different inoculum cell densities.

There was almost no expression of aggrecan mRNA at the initial time of differentiation culture (Fig. 1). Thereafter, the expression level increased monotonicaly until 168 h in all the cultures. At 72 h, the culture with the highest inoculation cell density showed the highest expression level. The aggrecan expression level in the culture with the lowest inoculum cell density was markedly lower than that of the other cultures at 168 h.

To confirm the presence of soluble factors produced by cells during the differentiation culture and the acceleration of the MSC differentiation, the conditioned media harvested on day 7 during the differentiation culture with the respective inoculum cell densities of 0.05 and 0.3×10^4 cells/cm^2 were employed for other differentiation cultures with the inoculum cell density of 0.3×10^4 cells/cm^2 for 3 d.

The aggrecan expression level in the culture using the conditioned medium from the culture with the initial cell density of 0.3×10^4 cells/cm^2 was markedly higher than that in the culture using the conditioned medium from the culture with the initial cell density of 0.05×10^4 cells/cm^2 (Fig. 2). It was also higher than the aggrecan expression level in the culture using the fresh medium.

It was revealed in previous experiments that a higher inoculum cell density results in a faster increase in the expression level of aggrecan mRNA during short-term culture such as 7 d. To confirm whether a higher inculum cell density leads to a higher expression level even in long-term culture, differentiation cultures with the inoculum cell densities

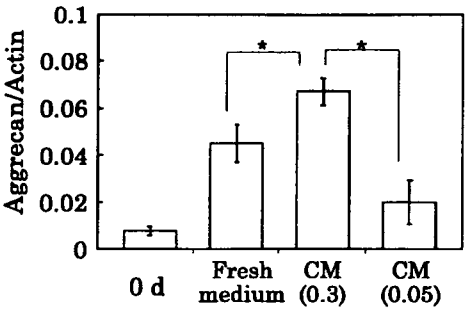

FIG. 2. Effect of conditioned medium on differentiation. Conditioned media were harvested at 7 d during the differentiation culture with inoculum cell densities of 0.05 and 0.3×10^4 cells/cm^2, respectively. Then, other differentiation cultures with an inoculum cell density of 0.3×10^4 cells/cm^2 for 3 d were performed employing fresh medium, and conditioned media from the cultures with inoculum cell densities of 0.05 (CM [0.05]) and 0.3×10^4 cells/cm^2 (CM [0.3]), respectively. Each bar indicates the standard deviation of triplicate culture. $P<0.05$.

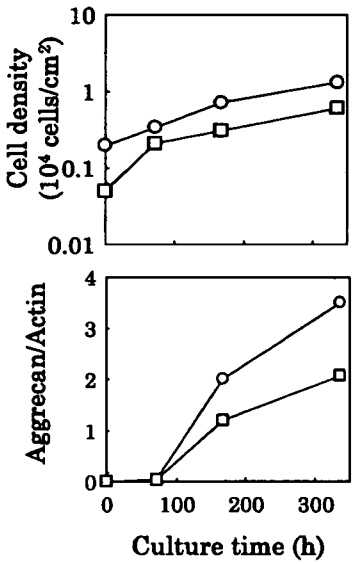

FIG. 3. Effect of inoculum cell density during long-term culture. The differentiation cultures with inoculum cell densities of 0.05 (squares) and 0.3×10^4 cells/cm^2 (circles) were performed for 14 d. Medium was changed weekly. The average of triplicate determinations is shown.

of 0.05 and 0.3×10^4 cells/cm^2 were performed for 14 d, with weekly medium changes.

The cells continued to grow until the end of culture (336 h) in both cultures with the inoculum cell densities of 0.05 and 0.3×10^4 cells/cm^2 (Fig. 3); there was no marked difference in growth rate between the cultures.

The aggrecan expression level at 169 h in the culture with the inoculum cell density of 0.3×10^4 cells/cm^2 was 1.69-fold that in the culture with the inoculum cell density of 0.05×10^4 cells/cm^2. Aggrecan expression level also continued to increase up to 336 h in both cultures. The expression level at 336 h in the culture with the higher inoculum cell density was also 1.69-fold that in the culture with the lower inoculum cell density.

The addition of TGF-β3 and IGF-1 initiated the differentiation of MSCs to chondrocytes, because almost no expression of aggrecan mRNA at 0 h of differentiation culture and a marked expression at 72 h were observed (Fig. 2). However, the expression level at 72 h differed between cultures with several inoculum cell densities in spite of the same concentrations of TGF-β3 and IGF-1 used. Thus, there might be factors other than TGF-β3 and IGF-1 affecting the expression of aggrecan mRNA in the culture. The other factors may not contain direct contact between cells, because the cultures did not reach confluence even at 168 h (data not shown). Moreover, the possible soluble factors may not affect cell growth rate, because the cell density employed in this study did not affect specific cell growth rate (Fig. 1).

The expression level of aggrecan mRNA reached 0.045 at 72 h with the use of fresh differentiation medium (Fig. 2), which was apparently lower than the expression level (0.26) at 72 h in the culture with the inoculum cell density of 0.3×10^4 cells/cm^2 obtained in an earlier experiment whose results are shown in Fig. 1. The reason for this difference may contain the difference in the condition of employed cells, because the expression level (0.022) at 0 h in the earlier experiment (Fig. 1) was higher than the expression level (0.008) in the later experiment (Fig. 2). However, the expression level in the culture using the conditioned medium from the culture with an initial cell density of 0.3×10^4 cells/cm^2 was markedly higher than those in both cultures using fresh medium and the conditioned medium from the culture with the initial cell density of 0.05×10^4 cells/cm^2 (Fig. 2). Consequently, the conditioned medium with the initial cell density of 0.3×10^4 cells/cm^2 might contain some soluble factors accelerating the increase in the expression level of aggrecan mRNA and the concentration of the possible soluble factors might be higher in the culture with the higher inoculum cell density. Not only the secretion of the soluble factors by cells but also the decomposition and inactivation of added factors such as TGF-β3 might occur during the culture. The later change may be dominant in the conditioned medium from the culture with the initial cell density of 0.05×10^4 cells/cm^2 and resulted in lower expression level compared with that with fresh medium. These may be the reason the expression level increased faster in the culture with the higher inoculum cell density (Fig. 1).

The concentration of soluble factors rather than cell density at each time during culture may affect the expression as mentioned above. Initial cell density might directly affect the time course of the concentration of the soluble factors. This may be the reason why the initial cell density apparently affected the increasing rate of expression level.

The concentration of cytokines produced in the cell culture was normally less than 1 ng/ml (2, 4). Thus, the possible soluble factors may be factors other than TGFβ3 and IGF1, whose concentrations in the fresh medium were 10 and 100 ng/ml, respectively.

The expression levels at 7 d (169 h) in the cultures with inoculum cell densities of 0.05 and 0.3×10^4 cells/cm^2 (1.19 and 2.02 in Fig. 3) were not so different from those at 7 d (168 h) in Fig. 1 (1.41 and 2.36), respectively. The fold increases in expression level due to the increase in the inoculum cell densities from 0.05 to 0.3×10^4 cells/cm^2 were 1.67 in Fig. 1 and 1.69 in Fig. 3, respectively. Thus, the effect of initial cell density on the increase in the expression level of aggrecan mRNA was quantitatively reproducible.

The fold increase in the expression level of aggrecan mRNA due to the increase in inoculum cell density from 0.05 to 0.3×10^4 cells/cm^2 was 1.69 at both 7 d (168 h) and 14 d (336 h) in Fig. 3. This shows that the effect of a higher inoculum cell density on the increase in the expression level was maintained for a long term such as 14 d. Besides, high inoculum cell density could reach to the same expression level (2.02 in Fig. 3) at 7 d as that (2.07 in Fig. 3) at 14 d in the culture with lower inoculum cell density. So, high inoculum cell density could decrease the length of culture period to the half that of lower inoculum cell density.

In conclusion, a higher inoculum MSC density accelerated the increase in the expression level of aggrecan mRNA in the differentiation medium supplemented with TGFβ3 and IGF-1. The fold increase caused by the higher inoculum cell density was quantitatively reproducible and maintained for at least 14 d. This effect may be due to some soluble factors produced by MSCs. Consequently, a higher inoculum MSC density might be appropriate for the differentiation of MSCs to chondrocyts for the regenerative therapy of cartilage.

REFERENCES

1. **Matsuda, C., Takagi, M., Hattori, T., Wakitani, S., and Yoshida, T.:** Differentiation of human bone marrow mesenchymal stem cells to chondrocytes for construction of three-dimensional cartilage tissue. Cytotechnology, **47**, 11–17 (2005).
2. **Takagi, M., Iemoto, N., and Yoshida, T.:** Effect of concentrations of murine stromal and hematopoietic cells on their three-dimensional coculture in nonwoven fabrics. J. Biosci. Bioeng., **94**, 365–367 (2002).
3. **Takagi, M., Nakamura, T., Matsuda, C., Hattori, T., Wakitani, S., and Yoshida, T.:** *In vitro* proliferation of human bone marrow mesenchymal stem cells employing donor serum and basic fibroblast growth factor. Cytotechnology, **43**, 89–96 (2003).
4. **Takagi, M., Horii, K., and Yoshida, T.:** Effect of pore diameter of porous membrane on progenitor content during a membrane—separated coculture of hematopoietic cells and stromal cell line. J. Artif. Organs, **6**, 130–137 (2003).

Appl Microbiol Biotechnol
DOI 10.1007/s00253-007-0897-9

BIOTECHNOLOGICAL PRODUCTS AND PROCESS ENGINEERING

Fetal calf serum-free culture of Chinese hamster ovary cells employing fish serum

M. Fujiwara · R. Tsukada · Y. Tsujinaga · M. Takagi

Received: 10 October 2006 / Revised: 15 February 2007 / Accepted: 19 February 2007

Abstract The effects of fish serum on cell growth and human granulocyte-macrophage colony-stimulating factor (hGM-CSF) production in an adhesion culture of Chinese hamster ovary (CHO) cells DR1000L4N were investigated and compared with those of fetal calf serum (FCS). Although fish serum did not stimulate the initial adhesion of CHO cells to culture dishes, it prompted cell growth after cell adhesion with FCS for 24 h. The cell density in the fish serum medium reached 75% that in the FCS medium. Fish serum promoted cell adhesion to and cell growth on collagen-coated dishes. The cell-specific production rate of hGM-CSF in the fish serum medium on collagen-coated dishes was almost the same as that in the FCS medium.

Keywords Fish serum · Fetal calf serum · Chinese hamster ovary cells

Introduction

Mammalian cell culture is an important and essential technology for pharmaceutical production and regenerative medicine. Cell adhesion and growth in culture generally require the addition of fetal calf serum (FCS) to the medium, because FCS can supply trace amounts of essential elements, such as hormones, vitamins, and growth factors. However, the use of FCS should be avoided owing to possible contamination by pathogens, such as prions derived from infected calves. Thus, the development of new useful substitutes in place of FCS is strongly desired. They are required to have high medical safety, that is, no-containing virulent factors for humans, and a comparable effect on cell growth with FCS.

No DNA or RNA viruses infecting fish have been reported to infect humans to date (Yoshimizu and Kasai 2005). Thus, employing fish serum in mammalian cell culture for medically related use is expected to be safe compared with employing FCS. However, the stimulating activities of fish serum for the adhesion and proliferation of mammalian cells are unknown.

Insulin-like growth factor I, insulin, growth hormone, and thyroxine were detected in the plasma of fish such as gilthead seabream (*Sparus aurata*; Funkenstein et al. 1989), coho salmon (*Oncorhynchus kisutch*; Larsen et al. 2001), Atlantic salmon (Nordgarden et al. 2005), and channel catfish (*Ictalurus punctatus*; Small and Peterson 2005). A complementary DNA (cDNA) encoding fibroblast growth factor 2 (FGF-2) has been isolated from the cDNA library of rainbow trout (Hata et al. 1997). A probable FGF was obtained from the swim bladder of red seabream (*Pagrus major*; Suzuki et al. 1994). Furthermore, primary cultures of cells from fish gills and kidneys were developed using serum from *Clarias gariepinus* (Rathore et al. 2001). Therefore, fish serum is expected to have some growth-stimulating effects on mammalian cells.

The Chinese hamster ovary (CHO) cell line is industrially important in the production of pharmaceutical proteins such as human granulocyte-macrophage colony-stimulating factor (hGM-CSF). In this study, the stimulatory effects of fish serum on the adhesion and proliferation of, and protein production by CHO cells were investigated and compared

M. Fujiwara · R. Tsukada · Y. Tsujinaga · M. Takagi (✉)
Division of Biotechnology and Macromolecular Chemistry,
Graduate School of Engineering, Hokkaido University,
North 13, West 8, Kita-ku,
Sapporo 060-8628, Japan
e-mail: takagi-m@eng.hokudai.ac.jp

with those of FCS. This study should be the first report of the application of fish serum for mammalian cell culture.

Materials and methods

Cells and media

hGM-CSF-producing CHO DR1000L4N cells were used. CHO DR1000L4N was constructed by transfecting CHO DG44 with the plasmid vector carrying the dihydrofolate reductase and hGM-CSF genes under the control of the SV40 promoter (Yoshikawa et al. 2000). Ham's F12-K medium (11.8 g/l; ICN, Aurora, OH) containing $NaHCO_3$ (2.25 g/l, Wako Pure Chemicals Industry, Osaka, Japan), 0.1 mg/ml streptomycin (Sigma, St. Louis, MO), and 100 U/ml penicillin (Sigma) was supplemented with 10% FCS (*v/v*) (26140-079; Gibco, Grand Island, NY) or fish serum (0–30%).

Fish serum

Fish blood was collected from a red seabream (*Pagrus major*; approximately 30 cm in body length, approximately 1 kg in body weight, farm raised in Ehime, Japan) using a syringe needle (23 G). The collected blood was left to stand for 2 h at room temperature and refrigerated at 4°C overnight. The fish blood was centrifuged (4°C, 3,000 rpm, 15 min) to remove blood clots, and the supernatant was filtered through a 0.22-μm membrane filter. The filtrate was stored at −20°C until medium preparation.

Cell culture

Cells were inoculated onto a 12-well plate (MS-80120; Sumilon, Tokyo, Japan) or a type I collagen-coated 12-well plate (4815-010; Iwaki, Tokyo, Japan) in a density range of $2–4\times10^4$ cells/cm^2 employing several media and then incubated at 37°C in an atmosphere containing 5% CO_2 for 24 h. Then, the cells were washed with phosphate-buffered saline, composed of 8 g/l NaCl, 0.2 g/l KCl, 1.15 g/l Na_2HPO_4, and 0.2 g/l KH_2PO_4, and further incubated for 48–72 h using several fresh media.

General analysis

The cell concentration in the culture was determined by nuclei staining, in which the adhering cells were incubated in a solution of 21 g/l citrate and 1 g/l crystal violet, and nuclei were counted under a microscope (Sanford et al. 1951). The hGM-CSF concentration in the culture supernatant was measured using an enzyme-linked immunosorbent assay kit (Pierce Endogen, Rockford, IL). Specific production rate of hGM-CSF ($q_{hGM\text{-}CSF}$) was calculated by the following equation:

$$q_{hGM-CSF} = \frac{1}{\overline{X}} \frac{dP}{dt} \quad (1)$$

Where $\overline{X}$ is the mean of the cell density and P is the increase in product (hGM-CSF) concentration during culture period for dt.

Results

Effects of fish serum on cell adhesion and growth

The effects of fish serum on cell adhesion and growth were studied (Fig. 1). CHO cells were inoculated onto the culture dishes with three types of medium containing 10% FCS, 10% fish serum, and no serum. Although the 10% FCS medium and serum-free medium resulted in cell-adhesion rates of 88 and 50% after 24 h, the 10% fish serum medium (25%) has a much lower cell-adhesion rate. The medium was changed to 10% fish serum medium at 24 h for one of the cultures in which cell inoculation was performed in 10% FCS medium, and cells grew even after the change. The cell density of the culture in which the medium was changed from 10% FCS medium to 10% fish serum medium reached 6.6×10^4 cells/cm^2 at 93 h, which was

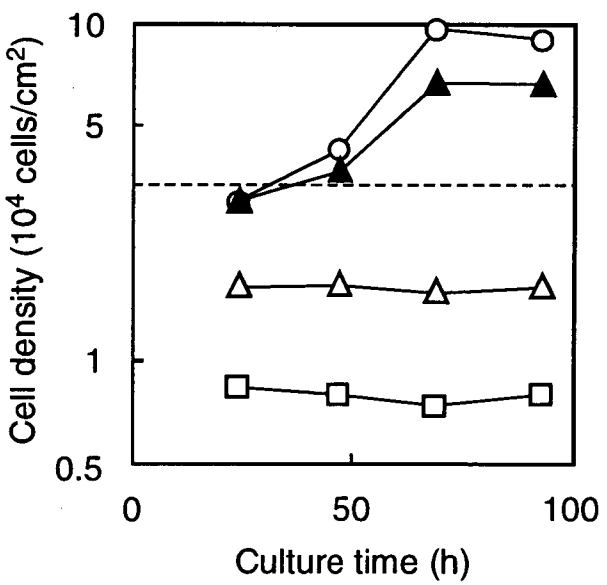

Fig. 1 Effects of fish serum on cell adhesion and growth of CHO cells. CHO DR1000L4N cells were inoculated onto media containing 10% FCS (*open circles*, *filled triangles*), no serum (*open triangles*), and 10% fish serum (*open squares*). The medium was changed from 10% FCS medium to 10% fish serum medium at 24 h (*filled triangles*). A *dashed line* represents the level of inoculum cell density (3.3×10^4 cells/cm^2). Data represent the mean of triplicate cultures